Machine Learning Approach to Compute Sensor Performance of Nanowire-based SPR Biosensor with Photonic Crystal Fiber

Submitted in partial fulfillment of the requirement
for the award of the degree of

Masters of Technology in Bioinformatics

Department of Applied Science

Indian Institute of Information Technology - Allahabad

Nitesh Kumar Dubey

MBI2020010

Under the guidance of:

Dr. Akhilesh Tiwari

The Academic Year 2021-2022

INDIAN INSTITUTE OF INFORMATION TECHNOLOGY,
ALLAHABAD
(A centre of Excellence in Information Technology Established by Govt. of India)

CANDIDATE'S DECLARATION

I, Nitesh Kumar Dubey, enrollment number: MBI2020010, certify that this thesis work entitled "**Machine Learning Approach to Compute Sensor Performance of Nanowire-based SPR Biosensor with Photonic Crystal Fiber**" is submitted by me in partial fulfillment of the requirement of the **Degree of Master of Technology** to the **Department of Applied Sciences, Indian Institute of Information Technology, Allahabad.**

I understand that plagiarism includes:

1. Reproducing someone else's work (fully or partially) or ideas and claiming it as one's own.

2. Reproducing someone else's work (Verbatim copying or paraphrasing) without crediting.

3. Committing literary theft (copying some unique literary construct).

I have given due credit to the original authors/sources through proper citation for all the words, ideas, diagrams, graphics, computer programs, experiments, results, and websites, that are not my original contribution. I have used quotation marks to identify verbatim sentences and given credit to the original authors/sources.

I affirm that no portion of my work is plagiarized. In the event of a complaint of plagiarism, I shall be fully responsible. I understand that my supervisor may not be in a position to verify that this work is not plagiarized.

Date: /06/2022
Place: IIIT Allahabad, Prayagraj

Nitesh Kumar Dubey
MBI2020010
M.Tech. Bioinformatics

INDIAN INSTITUTE OF INFORMATION TECHNOLOGY, ALLAHABAD
(A centre of Excellence in Information Technology Established by Govt. of India)

CERTIFICATE FROM SUPERVISOR

This is to certify that the statement made by the candidate is correct to the best of my knowledge and belief. The master's thesis titled "**Machine Learning Approach to Compute Sensor Performance of Nanowire-based SPR Biosensor with Photonic Crystal Fiber**" is a record of the candidate's work carried out by him under my guidance and supervision. I do hereby recommend that it should be accepted for the fulfillment of the requirements for the degree of **Master of Technology in Bioinformatics.**

Date: /06/2022
Place: IIIT Allahabad, Prayagraj

P

Dr. Akhilesh Tiwari
(Supervisor)
Department of Applied Sciences
IIIT Allahabad

INDIAN INSTITUTE OF INFORMATION TECHNOLOGY,
ALLAHABAD
(A centre of Excellence in Information Technology Established by Govt. of India)

CERTIFICATE OF APPROVAL

The forgoing thesis is hereby approved as a credible study in the area of Bioinformatics and its allied areas carried out and presented in a manner satisfactory to warrant its acceptance as a prerequisite to the degree for which it has been submitted. It is understood that by this approval the undersign does not necessarily endorse or approve any statement made, opinion expressed, or conclusion drawn therein but approve the thesis only for the purpose for which it is submitted.

Name and Signature of the Committee Members the on final examination for approval of the thesis.

ACKNOWLEDGEMENT

First and foremost, I want to convey my thanks to IIIT-ALLAHABAD. IIIT-A has given me the opportunity to acquire new approaches and concepts in order to improve my skills. Being a member of the IIIT-A family is the best asset I believe I have.

My mentor, **Dr. Akhilesh Tiwari**, was the most noteworthy source of advice. I owe him a debt of gratitude for giving me a novel concept. He has been my mentor throughout the thesis process. I'd want to express my gratitude for his insightful advice and support.

I'd want to offer my heartfelt gratitude and appreciation to **Mr. Ankur Gupta** for his invaluable assistance with my thesis.

I'd want to express my gratitude to my students and friends for their participation. Many people assisted and supported me during my thesis study, and I am grateful to them all.

This recognition would be inadequate without expressing my heartfelt gratitude to my family, without whom this thesis would not have been possible.

Nitesh Kumar Dubey

MBI2020010

June 2022

ABSTRACT

The bimolecular link is evaluated using Surface Plasmon Resonance (SPR). A popular topic is SPR detection based on Photonic Crystal Fiber (PCF). The detection efficacy of a Nanowire-based Multianalyte SPR Biosensor with Photonic Crystal Fiber (PCF), which includes the effective mode index and confinement loss, is quantified using a machine learning method in this work. For multiple analyte detection, SPRs are combined with geographically scattered multi-metal nanowires. The ANN method used in this study has excellent scalability and performance. Such machine learning algorithm which is based on artificial neural networks are capable of making precise estimates of the aforementioned optical characteristics for the typical dimensional space of wavenumber ranging from 0.5 to 0.8 um, pitch 1.9 um, refractive index for channels (ch1 and ch2) 1.33-1.38, and the number of cylinders 3. We show how feed-forward artificial neural networks can be used to anticipate results for uncertain device characteristics more quickly than using traditional computational methods. The processing runtimes needed for Lumerical MODE systems against neural networks (for training and validation) are also contrasted.

TABLE OF CONTENTS

LIST OF FIGURES

THESIS OUTLINES

Below mentioned are the outlines of my thesis chapter-wise:

Chapter 1: The first chapter gives an overview of SPR-based sensors with PCF, as well as the goal, purpose, and problem definition.

Chapter 2: The second chapter offers a summary of the literature review on PCFs, SPR sensors, and Computational works upon them.

Chapter 3: This chapter conveys the information about how data is simulated and analyses the data simulated with Comsol Software.

Chapter 4: This chapter tells about the methodology and the algorithm which I have used to accomplish the goal of this work. Also discusses the model implemented in this work.

Chapter 5: This chapter contains the findings of my approaches. It also discusses the accuracy and results obtained by model. It shows what are the runtimes of the model.

Chapter 7: This chapter includes the conclusion as well as potential future work.

CHAPTER 1: INTRODUCTION

The goal of this thesis is to compute the sensor performance of a bimetallic nanowire-based multi-analyte SPR biosensor with PCF. Using ANN, we can anticipate the optical characteristics of this detector with a precision of more than 98 cents. This chapter has covered the problem formulation, thesis goals, and thesis rationale. This chapter also explains the sensor's anatomy and its significance in the research domain.

1.1 Problem Definition

The optical properties of PCF-based sensors are computed by Conventional Lumerical Methods. This works by putting formulas using the Finite Element Method (FEM). The Conventional Lumerical Methods provide an accurate result. The Conventional Lumerical Methods require a huge amount of time and Computational power. In the fast-moving technology and fast-growing research, we require a tool that can reduce computational time and power. Machine Learning algorithms are a powerful way to get our goals accomplished.

1.2 Motivation

The goal of this study is to construct a machine learning technique that can more accurately predict and calculate the optical properties of a nanowire-based SPR biosensor using PCF. We are developing this method because the measurement of biomolecular association using the SPR sensing method has been an exciting area of study.

1.3 Objectives

Our main objectives are:

1) Simulate the data using the Finite Element Method (FEM) with Comsol Multiphysics.
2) Check the efficiency of the model by predicting the properties of the sensor using the GUI implemented in this work efficiently.

1.4 Introduction to Surface Plasmon Resonance (SPR) Biosensor

1.4.1 Surface Plasmon Resonance (SPR)

In the process known as surface plasmon resonance (SPR), electrons in the metallic outer surface are excited by photons of the incident beam that have a particular incident angle and subsequently move along to the surface of the metal. The refractive index of the substance close to the surface of the metal determines the angle upon which SPR is activated using a continuous light supply frequency and a thin metal layer [1]. As a practical matter, a slight modification to the detecting medium's reflecting index will lessen the occurrence of SPR and enable the detection of analytes.

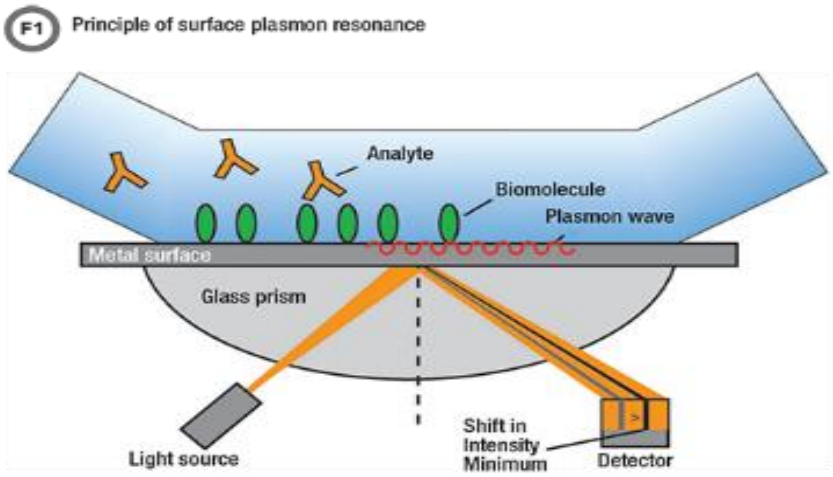

Figure 1.1 Principle of Surface Plasmon Resonance

1.4.2 What is a Biosensor?

The phrase "biosensor" was first used to represent the rapid identification of macromolecules at surfaces using transducer principles in the 1960s and 1970s. Such a well type of biosensor at the moment is the glucose sensor, which uses a specific enzymatic mechanism to report sugar levels in an electrical form, for

instance.

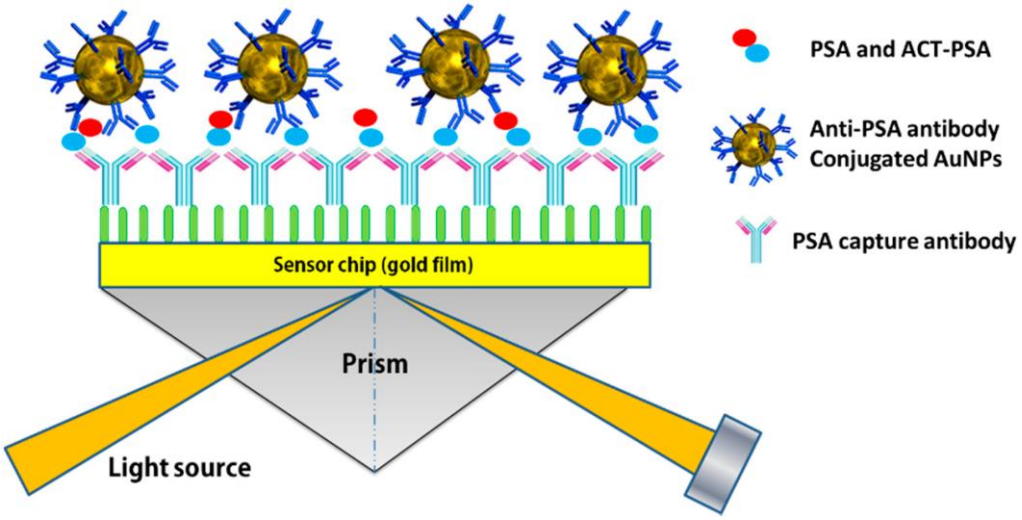

Figure 1.2 Example of SPR Biosensor

Surface plasmon resonance (SPR) biomarkers are one type of label-free photonic biosensing technology [2]. The visual evaluation of variations in index of refraction brought on by an analyte molecule connecting to biorecognized molecules immobilized on the SPR sensor in a collection forms the basis of the SPR method. Since the 1990s, SPR detection methods have been the main tool used in life science and pharmacological research to examine biomolecular relationships. Additionally, they are now being utilized quickly to identify biological and chemical particles in critical fields like ensuring food safety, pollution monitoring, and clinical applications.

1.5 Introduction to Photonic Crystal Fiber (PCF)

PCFs are a form of fiberoptic with a defective core that is either solid or hollow and a cyclical pattern of microcapillaries as the wrapping. Light dissemination and potential applications for PCFs have drawn a lot of attention since the mid-1990s (Russell, 2006) [3]. Photonic crystal fiber (PCF) is a three-dimensional FBG, a new form of optical fiber up of microscopic air holes in fiberglass. This enables it to confine light in hollow cores or with confinement properties not attainable in traditional optical fibers, particularly in nonlinear optics and high-power delivery [4]. The frequency shift on distinct scattering signals can be used to quantify temperature and strain simultaneously utilizing PCF in Brillouin scattering sensing.

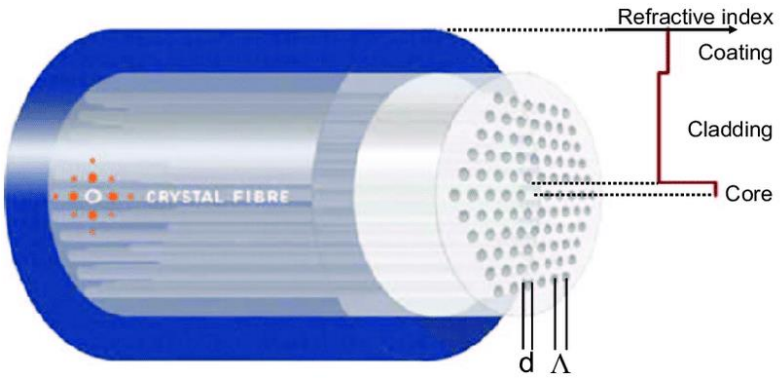

Figure 1.3 A solid core Photonic Crystal Fiber.

Modal region, chromatic aberration, discontinuities, and transmittance are just a few of the optical qualities that may be customised thanks to the innovation of the PCF structure and the variety of materials used in manufacturing. In a spectrum of uses, such as huge-mode-space infinitely solitary-mode fibers, aberration rectification, single polarisation, high birefringence navigation, and asymmetric ones, PCFs can perform much better than their conventional ones [5]. Typical applications include the creation of supercontinuum and beamforming, higher signal delivery in empty PCFs, high-power fiber lasers, and fiber components for spectrometry and measurement.

In the PCF coating and frequently in the center, the helical venules present a natural prospect for liquid substances to permeate them, either increasing their characteristics or offering a method of dynamic control.

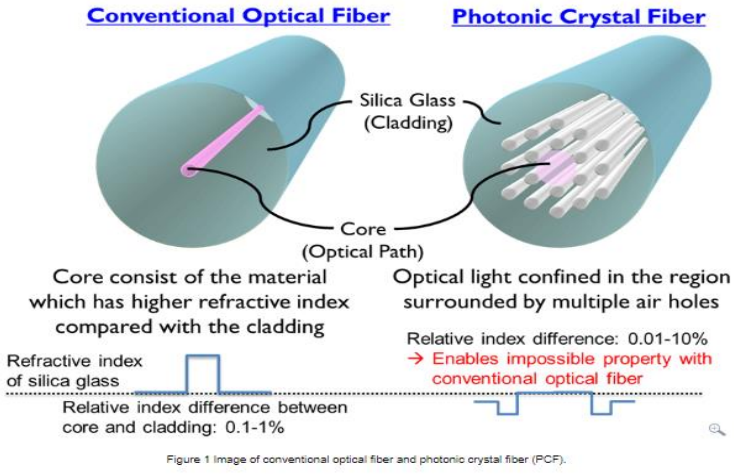

Figure 1.4 Conventional Optical Fiber vs Photonic Crystal Fiber

1.6 Introduction to Bimetallic nanoparticle and nanowire

A bimetallic nanoparticle is made up of two different metals that have been combined to produce a variety of new and better features. Bimetallic nanomaterials can be alloys, core-shell materials, or contact aggregates [6]. They've gotten a lot of interest from the scientific and industrial communities because of their unique features. When compared to monometallic cousins, they have higher activity when utilized as catalysts. They're low-cost, reliable alternatives with good activity and selectivity [7]. As a result, a great deal of work has gone into the development of these catalysts. The properties of metals are determined by the combination or type of metals present, how they are combined, and their size.

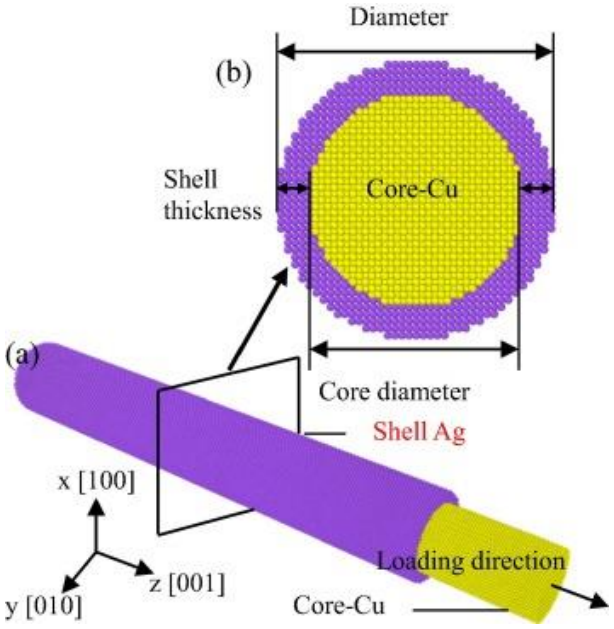

Figure 1.5 An Example of Bimetallic Nanowire (Copper Silver)

Because two different metals are joined, it is feasible to manipulate their properties to improve them. The bimetallic nanoparticle can be designed in a variety of ways for different applications [8]. For their synthesis and proper characterization, numerous approaches have been established. Bi-metallization improves electronic characteristics, which is the most important of the unique qualities. Charge transfer or orbital hybridization between the constituent metals are examples of electronic phenomena. Alloy formation can cause structural changes. During their synthesis, chemical and environmental conditions have a

role in determining their structural features [9]. The ultimate structural properties of the nanomaterial are determined by the differences in the reduction rates of several metal precursors.

1.7 Introduction to Bimetallic Nanowire-based Multi-analyte SPR Biosensor with PCF

This sensor combines two different metallic nanowires to create a juxtaposition of SPR for multi-analyte identification, which leads to efficient of the metallic layer production process. Using metal complexes increases the spectral bandwidth between both peaks [14]. The PCF is built using the stack and draw method. A surface plasmon resonance detector using bimetal nanorods for multianalyte monitoring is shown in Figure 5 using a photonic crystal fiber. To detect two ionic species, two distinct kinds of metallic nanorods are inserted

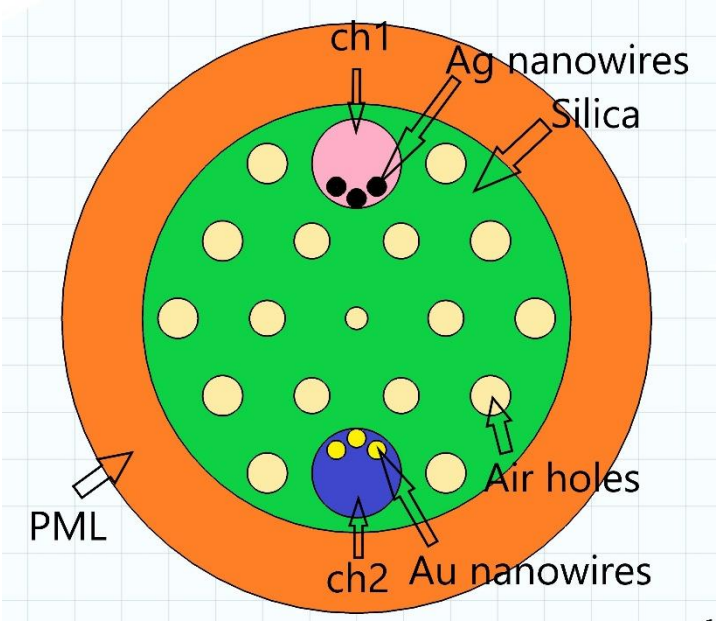

Figure 1.6 PCF based SPR multi-analyte Biosensor with Ag-Au nanowires

into the two large holes labeled ch1 and ch2. Ag nanorods comprising analyte 1 are present in the first channel, however Au nanorods carrying analyte 2 are present in the secondary channel [15]. A tiny air hole is made in the center to enhance the phase synchronization of the core mode and plasmonic mode. The first layer's diameter and pitch(which is 1.9um) factor are set to increase confinement loss, while the second layer's radii are somewhat bigger to improve

mode propagation. The second layer is made of two large pores that will allow metallic nanorods to be injected into the analytes. The selected sensor measures as follows: the two-layer hole pitching factor is 1.9 m, the small air air hole in the centre has radius 0.125 m, the first layer air hole has radius is 0.2 m, the second layer air hole radius is 0.225 m, and the two-channel hole radius 0.5 m. Surface plasmon generation requires Nnw = 3 nanowires [16]. Nanowire radius (rn) is 200 nm. Sellmeier's model predicts the RI of the fiber, which is formed of fused silica and varies on wavelength.

1.8 Introduction to Artificial Neural Network (ANN)

Artificial Neural Networks (ANN) are brain-inspired systems that would be used to foresee and anticipate complicated patterns [10]. A deep learning technique(approach) called the Artificial Neural Network (ANN) is based on the idea of biological neurons seen in the human psyche. The development of ANN was a result of an effort to replicate how the human brain processes. Biological neural networks and ANNs function similarly, despite not being exactly the same. The ANN classifier only accepts ordered, statistical values.

1.8.1 Architecture of Artificial Neural Network (ANN)

The input layer, the hidden layer (more than one), and the output layer are the three main levels that make up the network architecture. Because of the numerous levels, the MLP is commonly discussed (Multi-Layer Perceptron) [11]. The image below displays an ANN's layers.

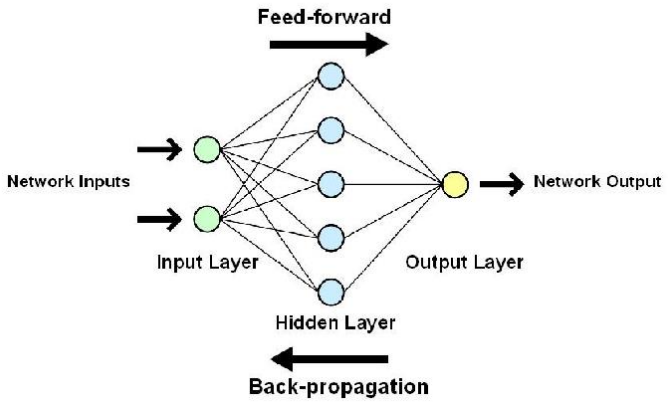

Figure 1.7 Architecture of an ANN

1. The hidden layer functions as a "fractionation layer," drawing out the most underlying features from the inputs and sending them to the following layer for additional examination. By detecting only the most significant information from the inputs and rejecting the redundant data, speeds up and enhances the network's efficiency.
2. For 2 purposes, the activation function is essential: first, it allows you to power on the machine, second,
    a. a. The presence of non-linear interactions between the inputs is captured by this model.
    b. b. It aids in the transformation of the input to a more useable output.

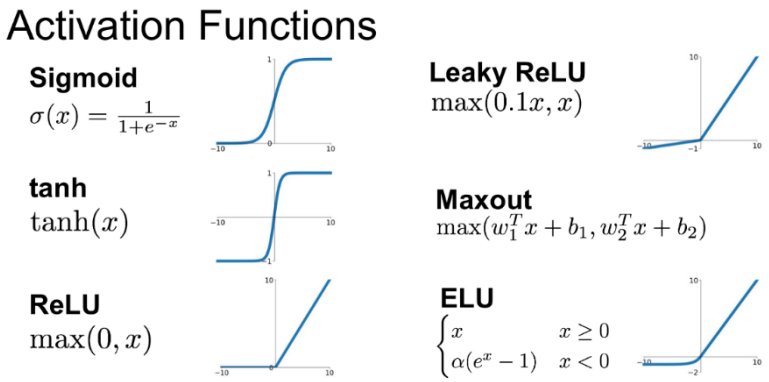

Figure 1.8 Activation Functions in ANN

3. Building a successful model requires finding the "optimal values of W — weights" that minimises prediction error. This is accomplished via the "backpropagation algorithm," which converts ANN into a learning algorithm by learning from mistakes [12].
4. To measure prediction errors, the optimization method employs a "gradient descent" technique. Small changes in W are explored to determine the best value for W, and the impact on prediction errors is examined. Finally, those W values are chosen as optimum since further W modifications have no effect on the number of errors.

CHAPTER 2: LITERATURE SURVEY

The bimolecular interaction is measured using the SPR sensing method. The Prism-based SPR sensor was utilized in the 1980s [13]. Prism was superseded by optical fiber in the nineties due to its vast dimensions and sparse commercial use in satellite imagery and remote detection. Phase synchronization of the two different modes and microfabrication encapsulation with PCF-based SPR detection were announced in 2006. Furthermore, coating layers of material within the fiber is a tricky problem that can be accomplished by D-shape and nanowire-based SPR sensors, despite the fact that nanowire-based SPR sensors lack the intricacy of fabricating layers of material.

To detect a single analyte in the past, only one plasmonic metal was employed. A metal-coated layer inside the fiber has also been used to produce many channels using just one plasmonic metal, enabling the detection of multiple analytes. Multi-molecule detection in an analyte and multi-sample detection of samples have both been accomplished via superposition of SPR utilizing D-shape PCF.

To model and optimize photonic crystal systems, computational techniques like the finite difference method, finite element method (FEM), block-iterative frequency-domain method, and plane wave expansion method are frequently utilized [17]. These methodologies require a significant amount of computational resources when working with difficult photonic crystal lattices that need to be replicated several times in order to arrive at an ideal design.

Computer vision, robots, virtual agents, and natural language processing are just a few of the fields where machine learning and deep learning have increasingly gained ground. The application and uses of machine learning

approaches in optical communications such as, multimode fibers, plasmonics, metamaterials, biosensing, metasurface design, optical communications, and networking, has also been a hot topics of recent studies and researches. Kiarashinejad et al. suggested a complexity reduction-based deep learning approach comprehend the characteristics of electromagnetic wave-matter interplay in nanostructures. Nanophotonics structures have also been studied using a geometric deep learning approach.

CHAPTER 3: SIMULATION AND DATA GENERATION

3.1 Simulation of data with Comsol Multiphysics

3.1.1 About Comsol Multiphysics

The multiphysics simulation modeling and finite element analysis programme COMSOL Multiphysics is cross-platform. It enables connected partial differential equations mechanisms as well as conventional science based user interfaces. COMSOL offers an IDE and a single methodology for electrical, mechanical, hydraulic, acoustical, and chemical applications. The foundational Multiphysics framework may solve PDEs in a weak form in addition to the common problems that application modules may address. An API for Java and LiveLink for MATLAB and Autodesk Inventor allow for the external influence of the applications. Self-contained tailored property-specific simulation apps can be made using an application builder.

3.1.2 Finite Element Method (FEM)

In order to do finite element analysis (FEA) on any physical phenomenon, one can use the finite element method (FEM), which is a numerical approach.

Mathematics is necessary to completely understand every physical process, including wave propagation, thermal transmission, architectural or fluid dynamics, and physiological cell growth. For most of these processes, partial differential equations are utilized as the description tool (PDEs). The finite element method, which was created in the last several decades, is one of the numerical techniques that has been used to enable computers to solve these PDEs.

Aeronautical and civil engineering both have a range of industrial applications. The capability of the applicability of the finite element approach is

only now starting to be fully realised. Among the most intriguing possibilities is its use in linked difficulties such as fluid-structure engagement, thermal - mechanical, thermolysis, and thermo-chemo-mechanical challenges, kinematics, bioengineering, piezoresistive, magnetoelectric, and electrodynamics.

3.1.3 Simulation of Data

The Bimetallic Nanowire-based SPR Biosensor with PCF is evaluated using COMSOL Multiphysics as a computational simulator. The Finite Element Method (FEM) and a precise free triangular mesh are used to numerically solve the wavefunction. The complicated propagation constant and confinement loss are calculated using a PML layer with anomalous absorption coefficient. Loss of confinement is,

$$CL(dB/cm) = 8.686 \times \frac{2\pi}{\lambda} Im(n_{eff}) \times 10^4$$

Where, Im(neff), in nm, is the imaginary portion of the transmission constant of the core mode at some specific wavelength. When the analyte's RI is altered, the plasmonic peak changes. The restrictions for this change are the follows:

$$S_\lambda(nm/RIU) = d\lambda_{peak}/dn_a$$

Sλ stands for spectrum susceptibility, and dλ(peak) is the change(variation) in resonant wavelength for a minute alteration in analyte d(na).

3.1.4 Analysis of Simulated Data

In order to evaluate the two analytes of which have (Refractive indexes)RI 1.33 and 1.37, the four permutations of RI of respective 2 channels are picked as indicated in Fig. 3 since it is believed that autoantibodies engagement caused the 0.01 change in RI of analytes.

Ch1 represents the communication of core mode potential with Ag nanowires, and Ch2 represents the connection of core mode power with Au nanowires. Two peaks have corresponding SPR wavelengths of 608nm and 728nm.

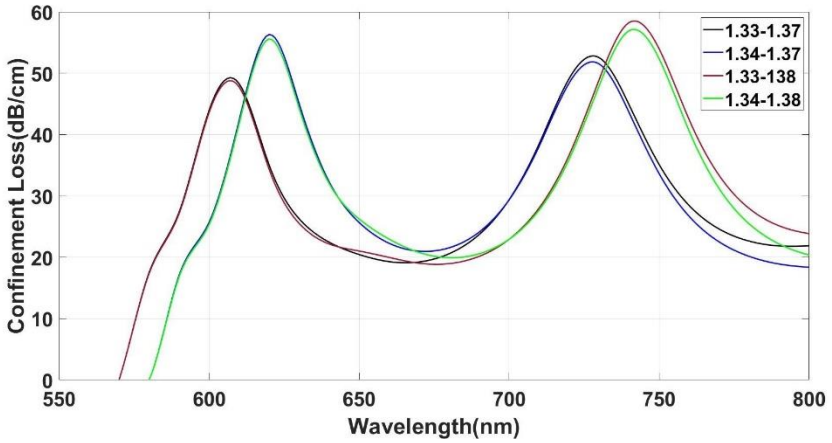

Figure 3.1. Confinement loss variations for different sets of channel analytes.

The last column in Fig. 3.2, which shows the data set produced by simulation, is for confinement.

Wavelength(nm)	Ref Index ch1	Ref Index ch2	Pitch(um)	Radius of core(r0)[um]	r hole radi	ir hole rad	l radius(R	f nanowire	nanowires	ode index	g(neff) [e	fLoss(dB/cm)
550	1.33	1.33	1.9	0.2375	0.38	0.4275	0.95	3	200	1.4516	0	0
555	1.33	1.33	1.9	0.2375	0.38	0.4275	0.95	3	200	1.4512	0	0
560	1.33	1.33	1.9	0.2375	0.38	0.4275	0.95	3	200	1.4509	0	0
565	1.33	1.33	1.9	0.2375	0.38	0.4275	0.95	3	200	1.4506	0	0
570	1.33	1.33	1.9	0.2375	0.38	0.4275	0.95	3	200	1.4502	0	0
575	1.33	1.33	1.9	0.2375	0.38	0.4275	0.95	3	200	1.4499	1.6254	15.4274
580	1.33	1.33	1.9	0.2375	0.38	0.4275	0.95	3	200	1.4496	1.9573	18.4174
585	1.33	1.33	1.9	0.2375	0.38	0.4275	0.95	3	200	1.4493	2.4293	22.6634
590	1.33	1.33	1.9	0.2375	0.38	0.4275	0.95	3	200	1.449	3.1002	28.6772
595	1.33	1.33	1.9	0.2375	0.38	0.4275	0.95	3	200	1.4486	4.005	36.7354
600	1.33	1.33	1.9	0.2375	0.38	0.4275	0.95	3	200	1.4483	5.0236	45.6945
605	1.33	1.33	1.9	0.2375	0.38	0.4275	0.95	3	200	1.448	5.7094	51.5033
610	1.33	1.33	1.9	0.2375	0.38	0.4275	0.95	3	200	1.4478	5.6095	50.1873
615	1.33	1.33	1.9	0.2375	0.38	0.4275	0.95	3	200	1.4475	4.9308	43.7564
620	1.33	1.33	1.9	0.2375	0.38	0.4275	0.95	3	200	1.4472	4.1818	36.8105
625	1.33	1.33	1.9	0.2375	0.38	0.4275	0.95	3	200	1.4469	3.6057	31.4854
630	1.33	1.33	1.9	0.2375	0.38	0.4275	0.95	3	200	1.4466	3.2286	27.9688
635	1.33	1.33	1.9	0.2375	0.38	0.4275	0.95	3	200	1.4463	3.0162	25.9231
640	1.33	1.33	1.9	0.2375	0.38	0.4275	0.95	3	200	1.446	2.9349	25.0272
645	1.33	1.33	1.9	0.2375	0.38	0.4275	0.95	3	200	1.4457	2.9631	25.0718
650	1.33	1.33	1.9	0.2375	0.38	0.4275	0.95	3	200	1.4454	3.0888	25.9344
655	1.33	1.33	1.9	0.2375	0.38	0.4275	0.95	3	200	1.4452	3.3037	27.527
660	1.33	1.33	1.9	0.2375	0.38	0.4275	0.95	3	200	1.4449	3.5948	29.7256
665	1.33	1.33	1.9	0.2375	0.38	0.4275	0.95	3	200	1.4446	3.9323	32.2719
670	1.33	1.33	1.9	0.2375	0.38	0.4275	0.95	3	200	1.4443	4.2582	34.6857
675	1.33	1.33	1.9	0.2375	0.38	0.4275	0.95	3	200	1.4441	4.4894	36.2981
680	1.33	1.33	1.9	0.2375	0.38	0.4275	0.95	3	200	1.4438	4.5506	36.5224

Figure 3.2 Snap of simulated data using Comsol Multiphysics

CHAPTER 4: METHODOLOGY

4.1 Flowchart

The figure depicted below gives an overview of the methodology applied in my work.

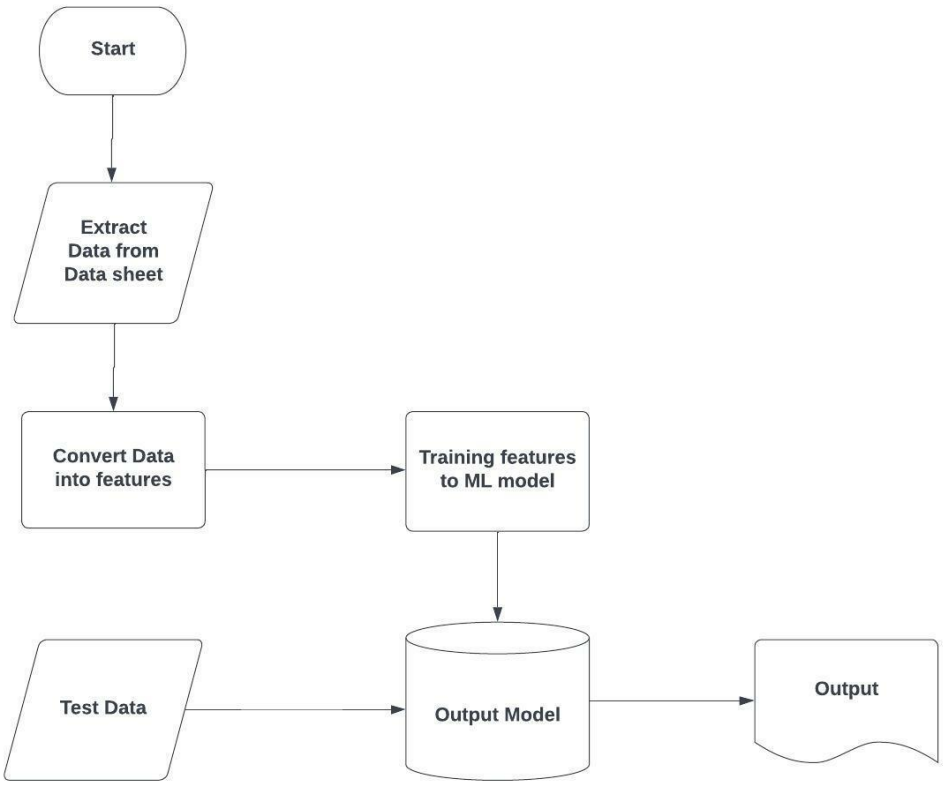

Figure 4.1: Flowchart

4.2 Modeling of the Sensor with ANN

In this part, the ANN/MLP architectural parameters, as well as the sensor used to generate the dataset, are discussed. A finite and appropriately labelled dataset is required for the initial step in the training method of an ANN model [18]. Any ANN model relies heavily on the dataset that was created initially. The prediction

accuracy is determined by how much the dataset is fitted to the issue to be addressed. The optical characteristics of several sensors were calculated after adjusting different Refractive Index values.

In our case, the labelled dataset was built using a set of sensor geometric data that included wavelength, refractive index of channel 1, refractive index of channel 2, pitch, radius of core, radius of layer 1 air hole, radius of layer 2 air hole, channel radius, number of nanowires, and radius of nanowire.

Following that, Lumerical Mode Solutions was used to compute neff and αc values for over 2000 samples, which are being used as the output variables of the labelled training dataset.

As shown in Fig. 4.2, the ANN/MLP model utilised in this study has 3 hidden levels with 50 nodes each. Each cluster or neuron in one layer is connected to the cluster or neuron in the level below, thanks to the entire interconnection of these hidden layers. 15% of the datapoints from the training sample were arbitrarily chosen to serve as the validation set, enabling objective assessment when adjusting the ANN variables (weights and biases). In order to estimate the non-linear function and weights to be optimized, accordingly, the Rectified Linear Unit (ReLU) activation function and the Adam optimizer were employed throughout the training procedure [19]. The ANN model makes certain outcome predictions after each cycle or epoch.

Based on the mean squared error (MSE) between the anticipated and measured outcomes, the back-propagation mechanism was used to adjust the hidden layer parameters for each epoch(iteration). The aforementioned factors were chosen using a hit-or-miss methodology for building the model and confirming the findings. For the PCF-based SPR sensor design under examination, three hidden layers, each one with 50 nodes, were discovered to be adequate for quickly establishing a stable MSE.

In order to reduce the computational load, we decided against introducing further layers and nodes. Another reason ReLU activation was adopted was because it performed better than Sigmoid and Tanh, two alternative non-linear activation functions (hyperbolic tangent) [20]. To increase the weighting factors

throughout the ML training stage, the Adam optimizer was chosen over LBFGS and stochastic gradient descent (SGD) optimizers since it also works well for a sizeable dataset. Once the MSE maintains a suitable value, the user decides how many epochs will be taken. We supply enough outcomes for the brand-new input data that wasn't provided all through the training stage after optimising the model with a steady MSE value [21].

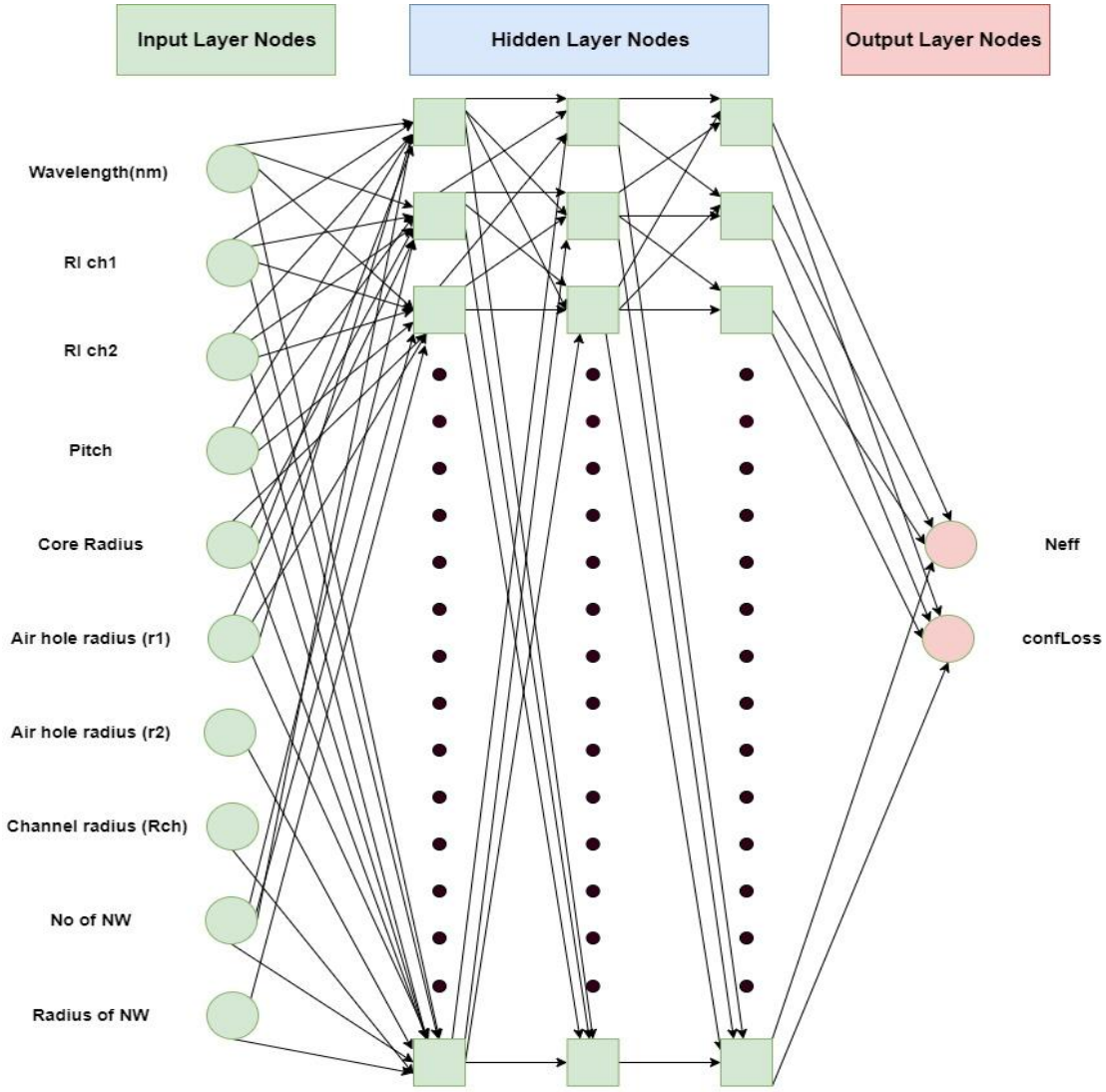

Figure 4.2: ANN representation with one input layer (10 input nodes), three hidden layers (50 nodes in each layer), and one output layer (2 output nodes).

CHAPTER 5: RESULTS AND ALGORITHMIC RUNTIMES

5.1 Effective Mode Index (Neff)

The result of effective mode index (neff) of the sensor computed by model, at epochs 1000, 2500 and 5000, is shown in this section. The scatter plots of Neff values from the dataset used in the training the ANN model are shown in the figures below. The prediction of Neff from the ANN model is compared to the actual value calculated from FEM simulations. A particular data point is represented by each circle. These circles should be lined closely to the straight y=x line in a well-trained model (black line).

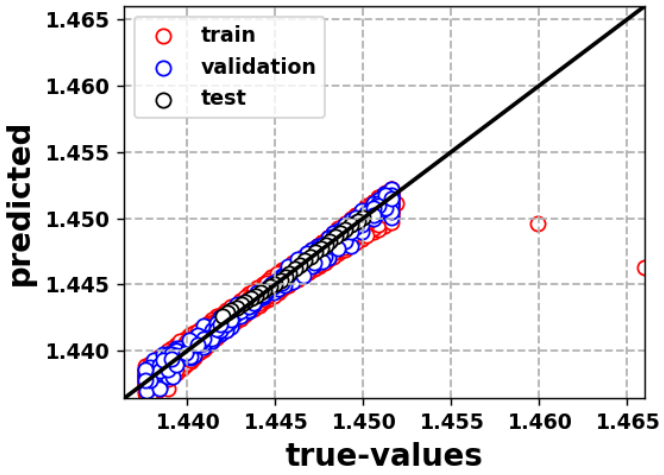

Figure 5.1: Predicted values vs true values of effective mode index(Neff) at epoch 1000.

We can see in Figure 5.1, that at epoch 1000, Neff points are not much close to the straight y = x line, the model couldn't train well at this amount of epoch. Also, we can see the MSE graph for training and validation points in Figure 5.2 at epoch 1000. The MSE curve is also not stabilized at this epoch. Model

is considered good if MSE is stable after increasing number of epochs.

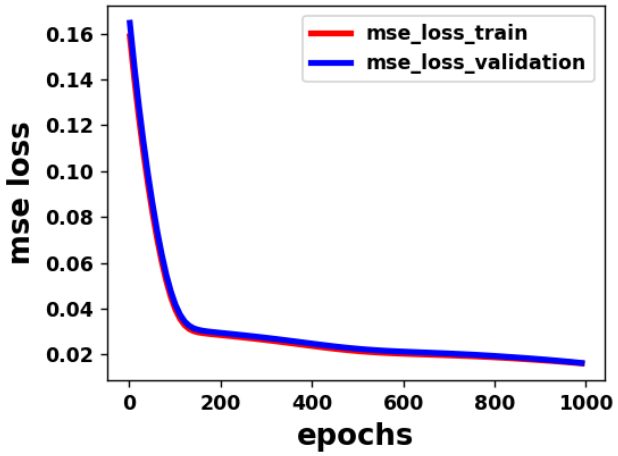

Figure 5.2: MSE Loss vs number of epochs for epochs 1000.

We can see that MSE loss decreases by increasing the number of epochs. MSE loss observed for epoch = 1 is 0.110931, for epoch 1000 MSE loss is 0.008942. In the Figure 5.3, Predicted values of Effective mode index (Neff) of shown against the simulated values.

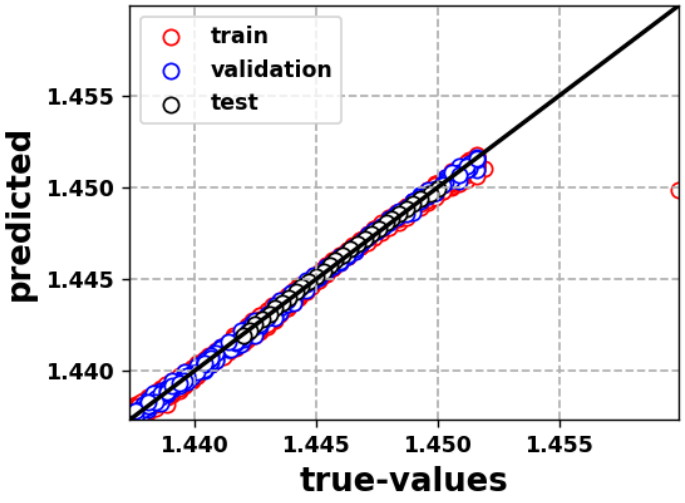

Figure 5.3: True values vs predicted values of Effective mode index (Neff) at epoch 2500

Running model for 2500 epochs gives better alignment compared to the result at epoch 1000. But the result obtained at epoch 2500 is that good as we can see the unstability in the Figure 5.4 as MSE loss is tending to be stable. Furthermore, the MSE loss observed at the end of 2500 epoch is 0.002718 but not stabilized yet.

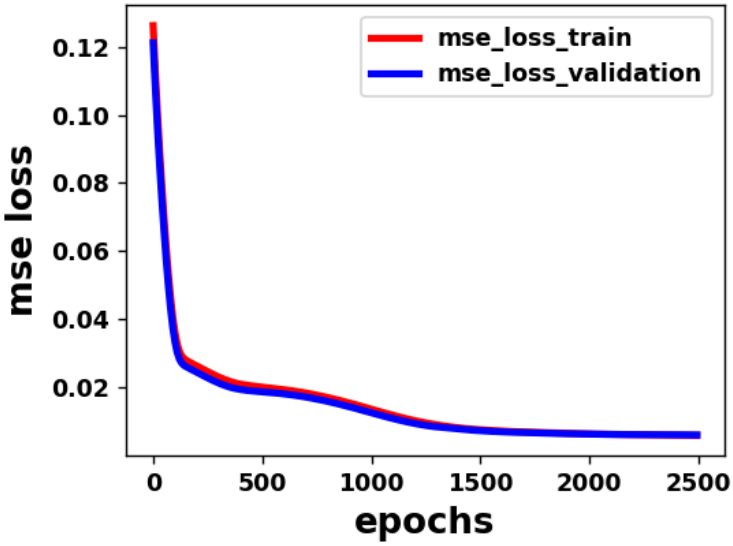

Figure 5.4: MSE loss vs number of epochs at epoch 2500

Next, we can see in the Figure 5.5, running the model for 5000 epochs gives the stable MSE and Neff is highly precise and aligned to y=x line very well. Stable value of MSE at epoch 5000 was 0.000646.

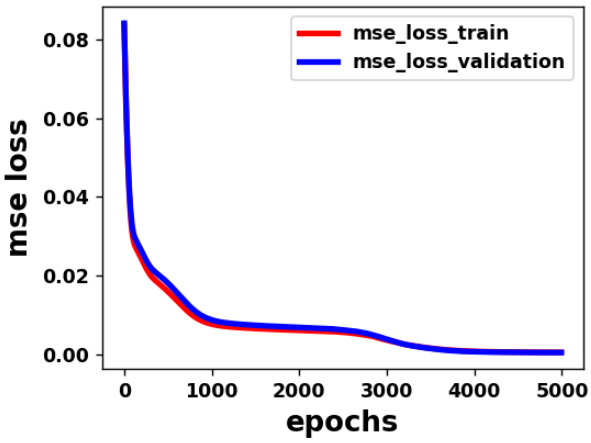

Figure 5.5 MSE loss vs epoch at epoch 5000

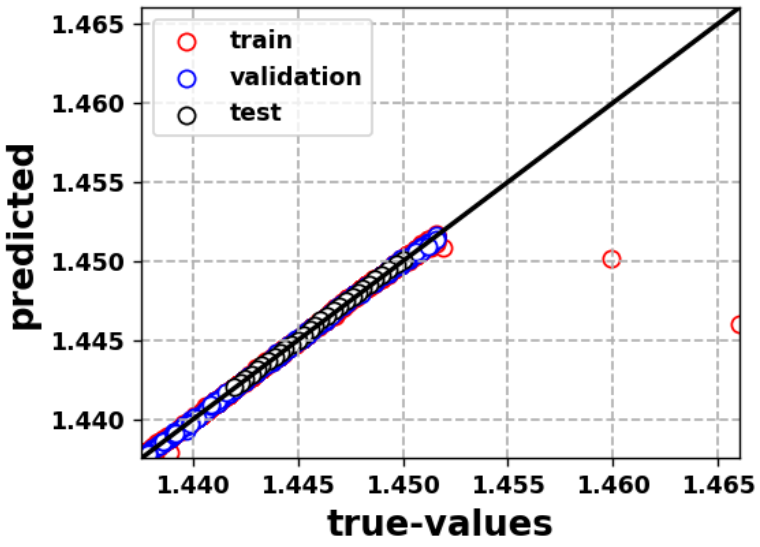

Figure 5.6 Actual values vs predicted values of Neff at epoch 5000

Running the model at 5000 epochs predicted accurate Neff with greater than 97% accuracy. We can see in Figure 5.6 that how predicted values are aligned with the actual values of Neff. This shows that 5000 epochs were enough to predict the values of Neff.

5.2 Confinement Loss (αc)

As we know that every photonic crystal fiber-based sensor has cons of confinement loss. Below Figures 5.7, 5.8 and 5.9 show the predicted values vs simulated values of confinement loss. At epoch 1000 the confinement loss predicted values are too scattered deviating from the y=x line which shows that 1000 epochs are not enough. While, running model for 2500 epochs we get a bit more accuracy. Running the model for 5000 epochs gives most accurate result as MSE loss gets stabilized and we can see in the Figure 5.9. The simulated vs predicted values are aligned closely to the y=x line.

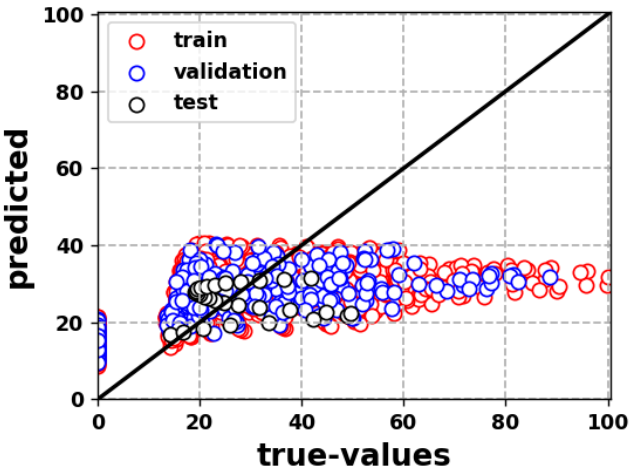

Figure 5.7 Predicted values vs simulated values of conf loss at epoch 1000.

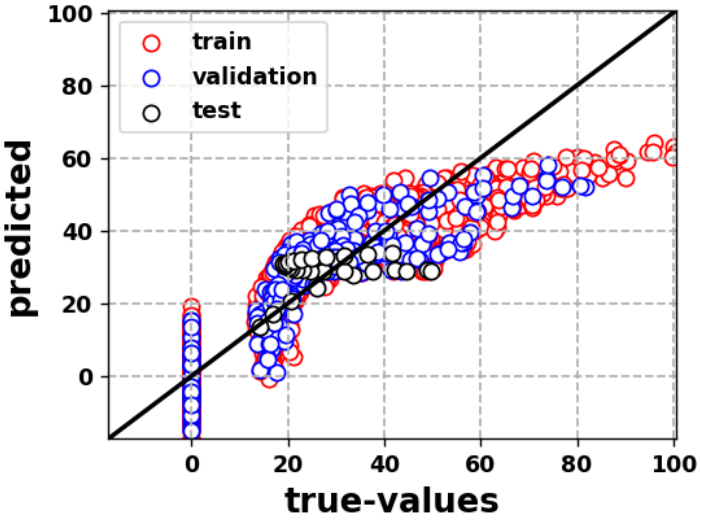

Figure 5.8 Predicted values vs simulated values of conf loss at epoch 2500.

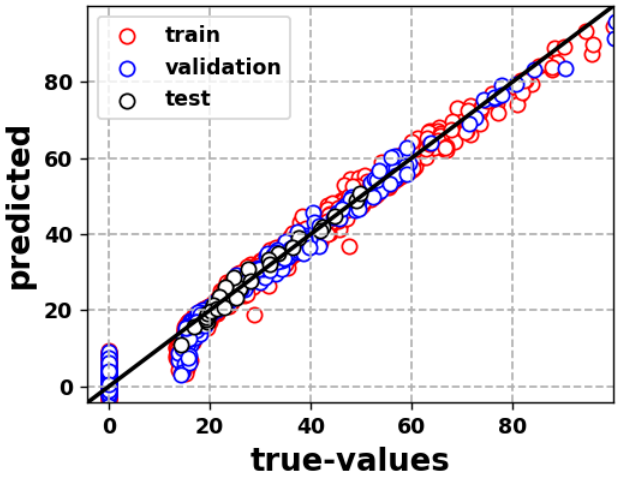

Figure 5.9 Predicted values vs simulated values of conf loss at epoch 5000.

5.3 Computational Performance

The Computer which was used in this work has following configurations:

Processor: Intel core i5 with 2.50 Ghz speed.

RAM: 8 GB of main memory

OS used: 64-bit Windows Operating System

The size of the dataset, the number of hidden layers, the number of nodes in each hidden layer, and the number of epochs used in training all affect the amount of time it takes to train the ANN model. The model used in this work has 3 hidden layers where each layer has 50 hidden nodes and it runs for 5000 epochs to give the best result. The total time taken in training of the time was around 30 seconds. To test and predict the optical properties of the described sensor the model took a few milliseconds.

While Lumerical Method requires around 2 minutes for each point to get calculated. Also, the machine required for the Lumerical Method is costly as most of the Lumerical method software requires high configuration machines.

CHAPTER 6: CONCLUSION AND FUTURE WORK

In conclusion, machine learning approaches were used to accurately forecast key features of a PCF-based sonsor design. This thesis demonstrates how, in contrast to numerical models, we can anticipate the effective mode index and confinement loss of a Nanowire-based multi-analyte SPR Biosensor with Photonic crystal fibre in milliseconds. Three hidden layers were employed throughout the code, with 50 nodes per level. This led to quick convergence and tolerable precision in forecasting outputs for the sensor's optical characteristics. As we can see from the mean squared error value decreasing with the number of epochs, the accuracy between the real and predicted points in estimating different optical attributes decreased as the batch size (iterations or epochs) rose. The machine learning models outlined above are believed to be effective and competent of enabling computing solutions for both forward and inverse problems. In the future, the code might be easily expanded to work with PCF-based sensors in addition to different core materials.

REFERENCES

1. J. C. Knight, T. A. Birks, P. St. J. Russell, and D. M. Atkin, “All-silica single-mode optical fiber with photonic crystal cladding,” Opt. Lett. 21(19), 1547–1549 (1996).
2. P. St. J. Russell, “Photonic crystal fibers: Basics and applications,” in Optical Fiber Telecommunications VA, (Elsevier, 2008), pp. 485–522.
3. W. J. Wadsworth, A. Ortigosa-Blanch, J. C. Knight, T. A. Birks, T.-P. M. Man, and P. St. J. Russell, “Supercontinuum generation in photonic crystal fibers and optical fiber tapers: a novel light source,” J. Opt. Soc. Am. B 19(9), 2148–2155 (2002).
4. M. R. Karim, H. Ahmad, and B. M. A. Rahman, “All-normal dispersion chalcogenide PCF for ultraflat mid-infrared supercontinuum generation,” IEEE Photonics Technol. Lett. 29(21), 1792–1795 (2017).
5. F. Benabid, J. C. Knight, G. Antonopoulos, and P. St. J. Russell, “Stimulated Raman scattering in hydrogen-filled hollow-core photonic crystal fiber,” Science 298(5592), 399–402 (2002).
6. F. Benabid, G. Bouwmans, J. C. Knight, P. St. J. Russell, and F. Couny, “Ultrahigh efficiency laser wavelength conversion in a gas-filled hollow core photonic crystal fiber by pure stimulated rotational Raman scattering in molecular hydrogen,” Phys. Rev. Lett. 93(12), 123903 (2004).
7. P. K. Cheo, A. Liu, and G. G. King, “A high-brightness laser beam from a phase-locked multicore Yb-doped fiber laser array,” IEEE Photonics Technol. Lett. 13(5), 439–441 (2001).
8. M. De, T. K. Gangopadhyay, and V. K. Singh, “Prospects of photonic crystal fiber as physical sensor: An overview,” Sensors 19(3), 464 (2019).
9. T. M. Monro, W. Belardi, K. Furusawa, J. C. Baggett, N. G. R. Broderick, and D. J. Richardson, “Sensing with microstructured optical fibres,” Meas. Sci. Technol. 12(7), 854–858 (2001).
10. R. Holzwarth, Th. Udem, T. W. Hänsch, J. C. Knight, W. J. Wadsworth, and P. St. J. Russell, “Optical frequency synthesizer for precision spectroscopy,” Phys. Rev. Lett. 85(11), 2264–2267 (2000).
11. A. da Silva Ferreira, G. N. Malheiros-Silveira, and H. E. Hernández-Figueroa,

"Computing optical properties of photonic crystals by using multilayer perceptron and extreme learning machine," J. Lightwave Technol. 36(18), 4066–4073 (2018).

12. Alireza Hassani and Maksim Skorobogatiy. Design of the microstructured optical fiber-based surface plasmon resonance sensors with enhanced microfluidics. Optics Express, 14:11616–21, 12 2006.
13. Ankur Gupta, Harpreet Singh, Ankit Singh, Rajat Kumar Singh, and Akhilesh Tiwari. D-shaped photonic crystal fiber–based surface plasmon resonance biosensors with spatially distributed bimetallic layers. Plasmonics, 18, 04 2020.
14. Ankur Gupta, Rohit Gadia, Ankit Singh, Rajat Singh, and Akhilesh Tiwari. Design analysis of multi sample-single analyte surface plasmon resonance biosensor based on d-shape photonic crystal fiber, 03 2021.
15. Gupta, A., Singh, A., Singh, R. K., & Tiwari, A. (2022, March). Bimetallic nanowire based multianalyte SPR biosensor with Photonic Crystal Fiber. In 2022 Workshop on Recent Advances in Photonics (WRAP) (pp. 1-2). IEEE.
16. Ying Lu, Cong-Jing Hao, Bao-Qun Wu, Xiao-Hui Huang, Wu-Qi Wen, Xiang-Yong Fu, and Jian-Quan Yao. Grapefruit fiber filled with silver nanowires surface plasmon resonance sensor in aqueous environments. Sensors, 12(9):12016–12025, 2012.
17. D. Pysz, I. Kujawa, Ryszard Stepien, M. Klimczak, Adam Filipkowski, Marcin Franczyk, L. Kociszewski, Jan Buzniak, K. Harasny, and Ryszard Buczynski. Stack and draw fabrication of soft glass microstructured fiber optics. Bulletin of the Polish Academy of Sciences: Technical Sciences, 62:667–682, 12 2014.
18. M. Bass and Optical Society of America. HANDBOOK OF OPTICS : Devices, measurements, and properties. McGraw-Hill, 1995.
19. T. Asano and S. Noda, "Optimization of photonic crystal nanocavities based on deep learning," Opt. Express 26(25), 32704–32717 (2018).
20. F. N. Khan, Q. Fan, C. Lu, and A. P. T. Lau, "An optical communication's perspective on machine learning and its applications," J. Lightwave Technol. 37(2), 493–516 (2019).
21. S. Chugh, S. Ghosh, A. Gulistan, and B. M. A. Rahman, "Machine learning regression approach to the nanophotonic waveguide analyses," http://dx.doi.org/10.1109/JLT.2019.2946572 (2019).

ORIGINALITY REPORT

9%	5%	7%	1%
SIMILARITY INDEX	INTERNET SOURCES	PUBLICATIONS	STUDENT PAPERS

PRIMARY SOURCES

1	Ankur Gupta, Ankit Singh, Rajat Kumar Singh, Akhilesh Tiwari. "Bimetallic nanowire based multianalyte SPR biosensor with Photonic Crystal Fiber", 2022 Workshop on Recent Advances in Photonics (WRAP), 2022 Publication	2%
2	www.simula.no Internet Source	1%
3	Sneha Verma, Sunny Chugh, Souvik Ghosh, B. M. Azizur Rahman. "Artificial Neural Network Modelling for Optimizing the Optical Parameters of Plasmonic Paired Nanostructures", Nanomaterials Internet Source	1%
4	Nazmi A. Mohammed, Omar E. Khedr, El-Sayed M. El-Rabaie, Ashraf A. M. Khalaf. "Literature Review: On-Chip Photonic Crystals and Photonic Crystal Fiber for Biosensing and Some Novel Trends", IEEE Access, 2022 Publication	<1%
5	en.wikipedia.org	